LANGMUIR Article
Cite This: Langmuir 2019, 35, 9934−9943
pubs.acs.org/Langmuir

# Comparing the Membrane-Interaction Profiles of Two Antiviral Peptides: Insights into Structure−Function Relationship

Soohyun Park,[†] Joshua A. Jackman,[‡] and Nam-Joon Cho*[,†,§]

[†]School of Materials Science and Engineering, Nanyang Technological University, 50 Nanyang Avenue 639798, Singapore
[‡]School of Chemical Engineering, Sungkyunkwan University, Suwon 16419, Republic of Korea
[§]School of Chemical and Biomedical Engineering, Nanyang Technological University, 62 Nanyang Drive 637459, Singapore

Supporting Information

**ABSTRACT:** In recent years, certain amphipathic, $\alpha$-helical peptides have been discovered that inhibit medically important enveloped viruses by disrupting the lipid membrane surrounding individual virus particles. Interestingly, only a small subset of amphipathic, $\alpha$-helical peptides demonstrate inhibitory activity, and there is broad interest in understanding how the structures of these peptides contribute to functional activity against lipid membranes. To address this question, herein, we employed multiple surface-sensitive measurement techniques along with computational simulations in order to investigate how AH and C5A peptides, two of the most biologically active peptides in this class, interact with model lipid membranes while gaining insight into membrane-induced peptide conformational changes. Circular dichroism spectroscopy experiments revealed that both AH and C5A peptides undergo pronounced coil-to-helix transitions in the presence of lipid membrane environments, and the C5A conformational change was the largest. Time-lapsed fluorescence microscopy measurements were conducted to monitor the interaction of peptides with arrays of tethered, individual lipid vesicles and showed that C5A potently lyses lipid vesicles indiscriminate of vesicle size at peptide concentrations as low as 10 nM whereas AH peptide preferentially lyses lipid vesicles with high membrane curvature and is less potent than C5A. These findings were complemented by electrochemical impedance spectroscopy measurements on a tethered lipid bilayer membrane platform, which indicated that C5A solubilizes lipid membranes in a manner that is distinct from how AH disrupts lipid membranes via pore formation. Computational simulations supported that the distinct membrane-interaction profiles arise from different helical folding patterns, whereby AH monomers predominantly exist as two shorter helices with a hinge in-between and C5A monomers form a single helix. Taken together, our findings demonstrate that membrane-active antiviral peptides can exhibit distinct membrane-interaction profiles that confer different degrees of targeting selectivity, and the corresponding structural insights will be useful for peptide engineering applications.

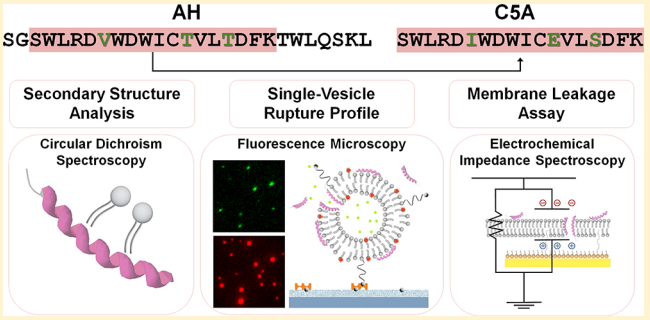


## INTRODUCTION

Membrane-active peptides are important anti-infective agents that target infectious pathogens by destabilizing phospholipid membrane coatings.[1−3] The classical description of anti-infective peptides typically focuses on cationic antimicrobial peptides that selectively destabilize membranes enriched in negatively charged lipids (e.g., bacterial cell membranes).[4,5] In recent years, there has been increased attention on another exciting class of anti-infective peptides termed antiviral peptides, which can directly impair the lipid membrane surrounding enveloped virus particles.[6] This antiviral approach has several compelling features, including broad-spectrum inhibitory potential against multiple classes of enveloped viruses, and there is a high barrier to the emergence of drug-resistant virus strains.[7,8] While the disruption of enveloped viruses by various classes of membrane-active agents (e.g., surfactants,[9,10] alcohols,[11] photosensitizers[12]) has long been known to reduce infectivity *in vitro*, recent evidence points to the *in vivo* and *ex vivo* efficacy of membrane-active antiviral peptides[13,14] and thus steps closer to realize potential translational opportunities. Together, these inhibitory activities have led to the paradigm concept of lipid envelope antiviral disruption (LEAD),[8] whereby an antiviral peptide-induced reduction in the extracellular concentration of infectious virus particles can lead to medically beneficial outcomes.

Within this scope, there is significant interest in understanding the basic design principles of membrane-active antiviral peptides, including how the structural properties of a peptide contribute to functional activity and the physicochemical basis of targeting selectivity.[13,15] Since the lipid membrane surrounding enveloped viruses is derived from host cell membranes, the lipid compositions of viral

Received: April 9, 2019
Revised: June 17, 2019
Published: July 10, 2019






DOI: 10.1021/acs.langmuir.9b01052
Langmuir 2019, 35, 9934−9943

membranes and infected cell membranes can be similar, and hence antiviral peptides need to have different mechanisms of targeting selectivity.[16] Unlike the cationic antimicrobial peptides described above, two of the most widely studied, membrane-active antiviral peptides, the 27-mer AH and 18-mer C5A,[17] have net charges of 0 and −2, respectively. Interestingly, the AH and C5A peptides have partially overlapping amino acid sequences and are both derived from the N-terminus of the hepatitis C virus (HCV) nonstructural protein 5A (NS5A), which plays an important role in HCV genome replication, as illustrated in Figure 1.

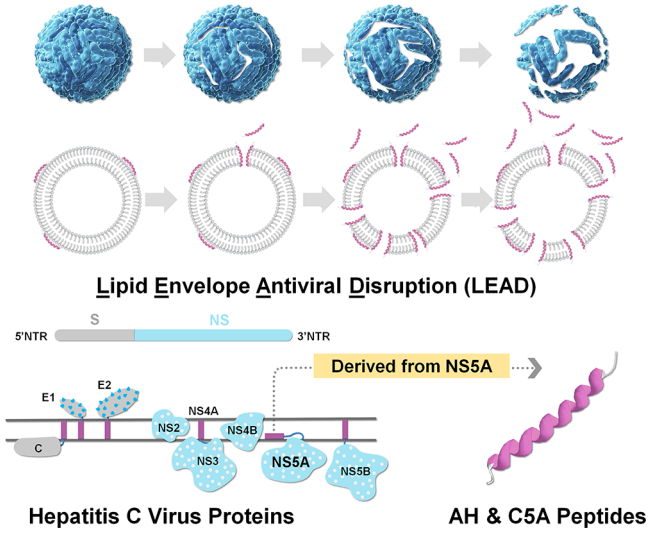


**Figure 1.** Schematic illustration of the LEAD concept and biological origin of the antiviral AH and C5A peptides, which correspond to the N-terminal amphipathic helix of the HCV NS5A protein.

Originally, the AH peptide was designed as a synthetic analogue to mimic the NS5A N-terminal amphipathic helix of an HCV genotype 1b strain (AH is an abbreviation for amphipathic, $\alpha$-helix) for at least two reasons: (i) NS5A membrane association is necessary for HCV genome replication and dependent on the NS5A N-terminus;[18] and (ii) it is difficult to express and purify full-length NS5A protein due to the amphipathic character of its N-terminus (it is often expressed without the N-terminus; see, e.g., refs 19−21). For these reasons, the AH peptide provided a useful model system to investigate the molecular determinants potentially influencing NS5A membrane association to model phospholipid and cell-derived membrane platforms.[22−24] In the course of these early studies, it was serendipitously discovered that the AH peptide can rupture lipid vesicles below a certain diameter (~160 nm; see refs 25 and 26), and follow-up studies indicated that this membrane-disruptive behavior relates to membrane-curvature-dependent pore formation and resulting strain-induced membrane lysis once a critical density of pores is formed.[25−28] In contrast to cationic antimicrobial peptides, the AH peptide has also been shown to disrupt lipid membranes largely independent of membrane surface charge.[29]

While it remains unclear how the membrane-disruptive activity of the isolated AH peptide might relate to supporting HCV genome replication, it has been demonstrated that the AH peptide's membrane-disruptive activity also works *in vitro* against numerous, medically important enveloped viruses such as Zika and Dengue along with HCV itself. Using various nanoscale characterization techniques, it has been shown that AH peptide treatment can disrupt virus particles in a similar manner to how it ruptures lipid vesicles.[25,30] Importantly, due to its membrane-curvature-dependent mechanism, AH peptide exhibits high potency against enveloped viruses (half-maximal efficacy in the range 10 nM to 1 $\mu$M depending on the virus and assay) while exhibiting low cytotoxicity against larger mammalian cells (half-maximal cytotoxicity around 50 $\mu$M or higher depending on the cell type and assay).[13] An engineered version of AH peptide that is composed of all D-amino acids was recently shown to work *in vivo* to therapeutically treat the lethal Zika virus infection in mice by reducing viral loads and blunting virus-related inflammation, and the peptide was also able to cross the blood−brain barrier.[13] While it is primarily thought that the AH peptide works against extracellular virus particles, it has been speculated that it might also inhibit intracellular NS5A membrane association through competitive binding to cellular receptors.[18]

A few years after the AH peptide was first designed, the C5A peptide was discovered through a high-throughput screen that investigated the potential anti-HCV activity of 441 synthetic peptides that were derived from the genome of an HCV genotype 1a strain.[17] Early work showed that the C5A peptide has potent antiviral activity against numerous enveloped viruses, including HCV, HIV, Dengue, and Herpes simplex (half-maximal efficacy in the range 500 nM to 5 $\mu$M depending on the virus and assay).[8,17,31,32] On the other hand, it was also reported that the C5A peptide exhibits greater hemolytic activity than the AH peptide,[15] and thus, its ongoing development has focused on topical microbicide applications. To date, the C5A peptide has been shown to protect mice[33] and nonhuman primates[14] against HIV transmission *ex vivo*. The current understanding is that the C5A peptide disrupts enveloped virus particles although it has also been shown to exhibit immune-stimulating activities, suggesting that it might be a useful adjuvant as well.[34] From a mechanistic perspective, an important distinction between the AH and C5A peptides is that the C5A peptide does not exhibit membrane curvature selectivity and ruptures lipid vesicles independently of vesicle size, which helps to explain why it has less targeting selectivity.[8,15]

At the same time, such functional differences motivate a deeper investigation of the membrane-interaction profiles of these two antiviral peptides, including clarifying how functional differences might be related to variations in peptide conformational structure and membrane-induced peptide conformational changes. Indeed, comparison of the aligned AH and C5A sequences reveals that the two peptides are structurally similar at the primary amino acid level and most amino acid differences between the two aligned sequences are conservative substitutions, which is consistent with the fact that the NS5A AH is conserved across HCV genotypes, including the 1a and 1b genotypes that have ~80% genetic similarity overall.[35,36] This similarity points to the likely importance of peptide conformational properties in driving membrane interactions and addressing this topic forms the focus of the present study.

Herein, using multiple surface-sensitive measurement techniques and computational simulations, we characterized the membrane-interaction profiles of AH and C5A peptides with model lipid membranes and sought to understand how peptide conformational changes drive these membrane interactions. Our experimental approach applied the nano-architectonics concept, whereby we selected two different


DOI: 10.1021/acs.langmuir.9b01052
*Langmuir* 2019, 35, 9934−9943

types of supported lipid membrane platforms, lipid vesicles with different degrees of membrane curvature, and a tethered lipid bilayer membrane (tBLM), in order to characterize the membrane−peptide interactions using different measurement techniques.[37−40] To this end, circular dichroism spectroscopy experiments were conducted to determine peptide secondary structure in aqueous buffer and in the presence of lipid membrane environments, leading to insights into coil-to-helix folding and the thermodynamics of membrane−peptide interactions. These results were complemented by single-vesicle assay measurements to characterize the real-time interactions of the two peptides with lipid vesicles along with electrochemical impedance spectroscopy measurements to determine to what extent the peptide interactions cause membrane leakage in the tBLM configuration. Together, these experimental studies build a comprehensive picture of how AH and C5A peptides distinctly interact with lipid membranes, and additional computational simulations further provided insight into how these functional differences might relate to peptide conformational structure.

## EXPERIMENTAL SECTION

**Reagents.** High-purity AH and C5A peptides (96% and 95%, respectively) were synthesized by AnaSpec Corporation (Fremont, CA, USA). The lyophilized peptide was weighed and solubilized in deionized water to prepare a highly concentrated stock concentration (2 mg/mL). The molar concentrations of the two peptides were determined by absorbance measurements at 280 nm wavelength, and a Boeco-S220 spectrophotometer (Boeco, Hamburg, Germany) was used for the experiments.[41] The experimentally determined molar concentrations of AH and C5A peptides were 554 and 782 $\mu$M, respectively, which indicate that both peptides have a high solubility in water. The peptide stock aliquots were stored at −20 °C and diluted in buffer solution before the experiments. Lipids were obtained from Avanti Polar Lipids (Alabaster, AL, USA) and were supplied as a dispersion in a chloroform solution or in a lyophilized, powder form. Lipids included 1,2-dioleoyl-*sn*-glycero-3-phosphocholine (DOPC) for all experiments, and 1,2-distearoyl-*sn*-glycero-3-phosphoethanolamine-*N*-[biotinyl(polyethylene glycol)-2000] (ammonium salt) (DSPE-PEG(2000)biotin) and 1,2-dioleoyl-*sn*-glycero-3-phosphoethanolamine-*N*-(lissamine rhodamine B sulfonyl) (ammonium salt) (Rh-PE) were used for tethered vesicle experiments. All of the lipid reagents were mixed in chloroform to the desired molar ratio before vesicle preparation as described below. The aqueous buffer was 10 mM Tris [pH 7.5] buffer with 150 mM NaCl unless otherwise noted. All solutions were prepared using Milli-Q-treated water (MilliporeSigma, Burlington, MA, USA).

**Circular Dichroism (CD) Spectroscopy.** The secondary structure of peptides was characterized by CD spectroscopy experiments using a Chriascan spectropolarimeter (Model 420, AVIV Biomedical Inc., Lakewood, NJ, USA) with a 0.1 cm path length cuvette (Hellma GmbH, Müllheim, Germany). The test peptide concentration was fixed at 100 $\mu$M. Mixtures of peptide and lipid were mixed to the appropriate concentration (for example, a P:L ratio of 1:10 corresponds to 100 $\mu$M peptide and 1 mM lipid in the sample mixture) and then incubated for 30 min before experiment. The aqueous buffer used for all steps was 10 mM Tris [pH 7.5] buffer with 150 mM NaCl. The maximum lipid concentration was set at 2 mM, which is within the optimal range for data collection.[42] Spectral data were collected in triplicate at 25 °C, and the wavelength range was 190−260 nm with 1 nm bandwidth, a step size of 0.5 nm, and a time constant of 0.1 s. Background scans without peptide were recorded using the same conditions and subtracted accordingly. The final averaged spectra were calculated in mean residue molar ellipticity units ($[\theta = \theta/10 \times c \times l]$), where $\theta$ is the ellipticity, $c$ is the molar concentration of peptide, and $l$ is the path length in centimeter. The presented spectra were smoothed by the Savitzky−Golay method with a polynomial order of 2. The fractional helicity (fH) of the peptides was calculated as follows

$$\mathrm{fH} = \frac{[\theta]_{222}^{\mathrm{Obs}} - 3000}{-36000 - 3000}$$

where $[\theta]_{222}^{\mathrm{Obs}}$ is the molar ellipticity at 222 nm.[15,43]

**Tethered Vesicle Platform.** Glass coverslips (ibidi GmbH, Martinsried, Germany) were cleaned and treated with oxygen plasma (model PDC-002, Harrick Plasma, Ithaca, NY, USA) for 30 s, before being assembled in a microfluidic chamber (sticky slide VI 0.4, ibidi GmbH). The coverslips were then coated with a mixture of 50/50 wt % poly(L-lysine)-grafted poly(ethylene glycol) (PLL-*g*-PEG) and poly(L-lysine)-grafted poly(ethylene glycol)-biotin (PLL-*g*-PEG-biotin) (SuSoS AG, Dübendorf, Switzerland) at a polymer mass concentration of 41.5 $\mu$g/mL. The incubation time was 30 min followed by a rinse in 10 mM Tris [pH 7.5, 150 mM NaCl] buffer. Then, the surface was incubated with 0.17 $\mu$M neutravidin for 5 min, followed by buffer washing. Biotinylated vesicles were next immobilized on the functionalized surface by biotin-neutravidin coupling at a lipid concentration of ∼0.03 $\mu$M. Image analysis was performed using ImageJ software (National Institutes of Health, Bethesda, MD) and an in-house software program written in Python code, as previously described.[15]

**Vesicle Preparation.** For a tethered vesicle platform, small unilamellar vesicles (SUVs) were prepared by the extrusion method, as previously described.[44] Dissolved lipids (99.2 mol % DOPC, 0.7 mol % of Rh-PE and 0.1 mol % of DSPE-PEG(2000)biotin) in chloroform were first dried under a gentle stream of nitrogen gas at room temperature and were then stored under vacuum conditions overnight to remove any remaining chloroform by evaporation. Multilamellar vesicles were then generated by hydrating and vortexing the dried lipids in aqueous buffer to achieve a bulk lipid concentration of ∼2.5 mM. The buffer contained 14.3 mM calcein dye (maximum excitation and emission wavelengths of 494 and 517 nm, respectively), which was thus incorporated into the lipid vesicles. After hydrating the lipid samples, the vesicles were subjected to seven cycles of freeze−thaw treatment to increase encapsulation efficiency and unilamellarity. Then, the lipid suspension was repeatedly passed through a polycarbonate filter a total of 11 times by using a MiniExtruder (Avanti Polar Lipids). Depending on the diameter of pores within the filter, the average diameter of extruded vesicles was 126 and 313 nm for 100 and 400 nm filters, respectively, as determined by dynamic light scattering (Figure S1). The as-prepared vesicle suspensions were diluted before the experiments to a lipid mass concentration of ∼0.25 mM, and nonencapsulated calcein was removed by a Sephadex G-25 gel filtration column (GE Healthcare Life Sciences, Pittsburgh, PA, USA).[45]

**Epifluorescence Microscopy.** Imaging experiments were conducted using a Nikon Eclipse Ti-E inverted microscope with a 60× oil-immersion objective (NA 1.49). The excitation source was a mercury-fiber illuminator C-HGFIE Intensilight (Nikon, Tokyo, Japan), and the light was passed through an alternating dichroic filter block (Ex 480/40, Em 535/50) or (Ex 545/30, Em 605/70) for imaging in the FITC and TRITC channels, respectively. An Andor iXon3 897 EMCCD camera (Andor Technology Ltd., Belfast, United Kingdom) was used to record images at a rate of 1 frame per 0.2−0.4 min in four neighboring spots. The experimental substrate was enclosed within a microfluidic chamber, and the liquid sample was introduced at a flow rate of 100 $\mu$L/min, as controlled by a peristaltic pump (model no. ISM833C, Ismatec, Wertheim, Germany). All measurements were conducted at room temperature (∼25 °C).

**Electrochemical Impedance Spectroscopy (EIS).** The EIS measurement platform consisted of gold electrodes that were supplied by SDx Tethered Membranes (Roseville, New South Wales, Australia) and coated with 10 mol % tether (benzyl disulfide octoethylene glycol phytanyl) and 90 mol % spacer (hydroxyl terminated benzyl disulfide tetra-ethylene glycol) molecules dispersed in ethanol. The assembled tethaPlate (SDx Tethered Membranes) contained six flow cells with a 2.1 mm$^2$ electrode surface area per cartridge, and the



DOI: 10.1021/acs.langmuir.9b01052
*Langmuir* 2019, 35, 9934−9943

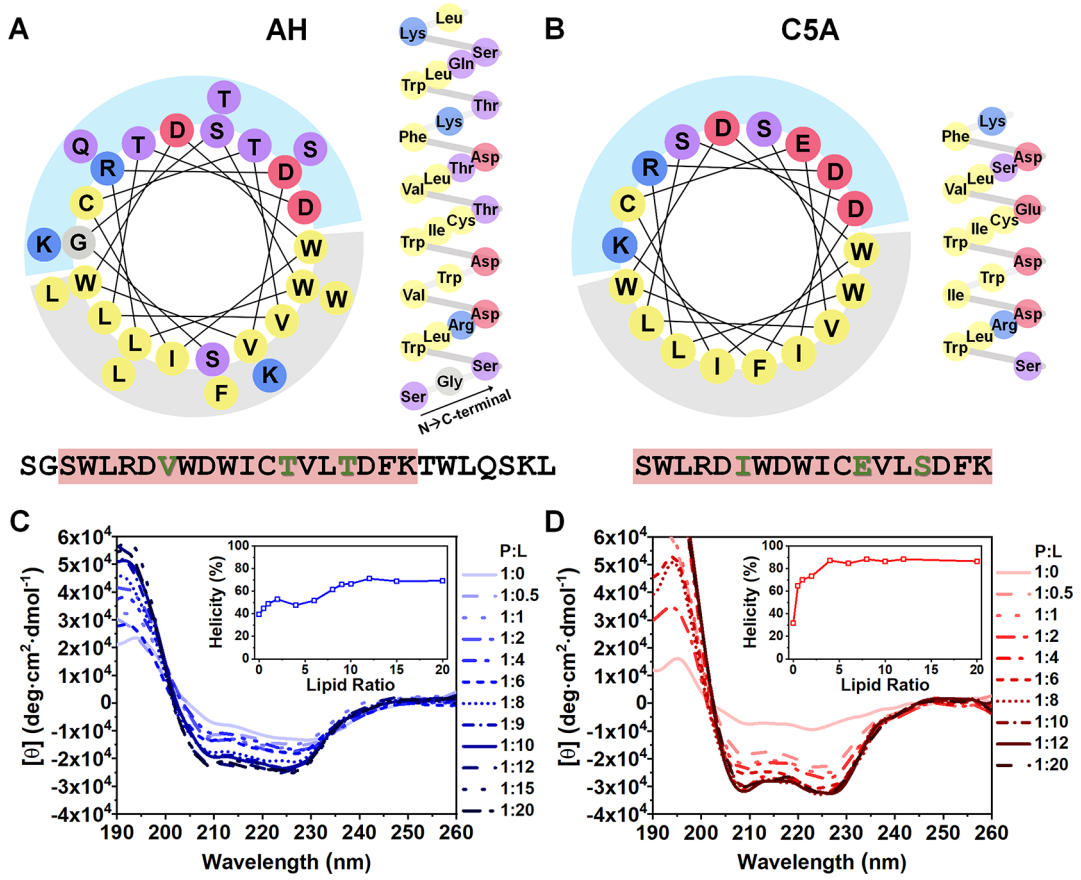


**Figure 2.** Secondary structure comparison of AH and C5A peptides. Helical wheel projection of (A) AH and (B) C5A amino acid sequences showing an amphipathic distribution of hydrophilic (purple), positively charged (blue), negatively charged (red), and hydrophobic (yellow) amino acid residues. Circular dichroism (CD) spectroscopy analysis of (C) AH and (D) C5A peptides in the presence of lipid concentrations (with fixed peptide concentration of 100 $\mu$M). Insets show the fractional helicity percentages of the two peptides as a function of normalized lipid concentration (defined as lipid concentration over peptide concentration; a value of 20 on the *x*-axis insets corresponds to 2000 $\mu$M lipid, for example). All presented spectra were obtained by averaging three technical replicates, and the helicity percentages were calculated on the basis of the mean ellipticity values at the 222 nm wavelength.

formation of tethered bilayer lipid membranes (tBLMs) on the sensor surfaces was initiated by the addition of 8 $\mu$L of 3 mM DOPC lipid in ethanol. After 2 min of incubation, the flow cell was rapidly rinsed with 10 mM Tris [pH 7.5, 150 mM NaCl] buffer (3 cycles × 100 $\mu$L per cycle) in order to promote tBLM formation. Afterward, 100 $\mu$L of the appropriate test sample was injected into each well. TethaPod and tethaPatch units from SDx Tethered Membranes were used as the membrane conductance and capacitance reader and as the potentiostat connectivity unit, respectively. All measurements were collected under ambient room-temperature conditions (~25 °C) and analyzed using the tethaQuick software program (SDx Tethered Membranes), as previously described.[46,47]

**Structural Modeling.** The conformational properties of free peptide molecules in bulk solution were predicted by using the PEP-FOLD3 server, which is an online computational framework for *de novo* structural modeling.[48] The simulations were conducted without any preset data; i.e., the modeling was unbiased. Structural prediction occurs in three consecutive steps: (1) the peptide structure is described by a series of fragments of four amino acids, overlapping by three amino acids each; (2) conformations are generated on the basis of the prototype fragments followed by optional refinement with a Monte Carlo procedure; and (3) predicted conformations are ranked according to a scoring system.[49] The predicted conformational structures of free peptide monomers were visualized using the Swiss-PdbViewer program.[50]

**Statistical Analysis.** Statistical analysis was performed using the Origin 2018 software package (OriginLab, Northampton, MA, USA). The number of vesicles analyzed per sample was typically >300. The mean ± standard deviation (sd) in histogram plots was determined by Gaussian fitting, and sd was defined as fwhm/2.355, where fwhm is the full-width-at-half-maximum.

## RESULTS AND DISCUSSION

**Secondary Structure Characterization.** In Figure 2A,B, the helix net projections and amino acid sequences of the AH and C5A peptides are presented and show the amphipathic disposition of each peptide, as indicated by polar (blue) and nonpolar (gray) faces. A small disturbance in the AH peptide's amphipathicity is noted due to polar residues being introduced near each end of the nonpolar face (S1 and K26 in the N- and C-terminus, respectively). The 18-mer C5A peptide is related to the middle section of the 27-mer AH peptide with 3 amino acid differences that are highlighted in green. These differences represent conservative mutations that arise from substituting nonpolar with nonpolar (V8 to I6) or polar with polar (T14 to E12, T17 to S15) residues and relate to the different genotypic origins of the two peptides as discussed in the Introduction. As such, both peptides have similar near-neutral electrical properties, and the net charges of the AH and C5A peptides are 0 and −2, respectively. Likewise, the hydrophobicity ($H$) of each peptide was comparatively high (0.69 and 0.74, see Table S1). Hence, the primary amino acid sequences of the AH and



DOI: 10.1021/acs.langmuir.9b01052
*Langmuir* 2019, 35, 9934−9943

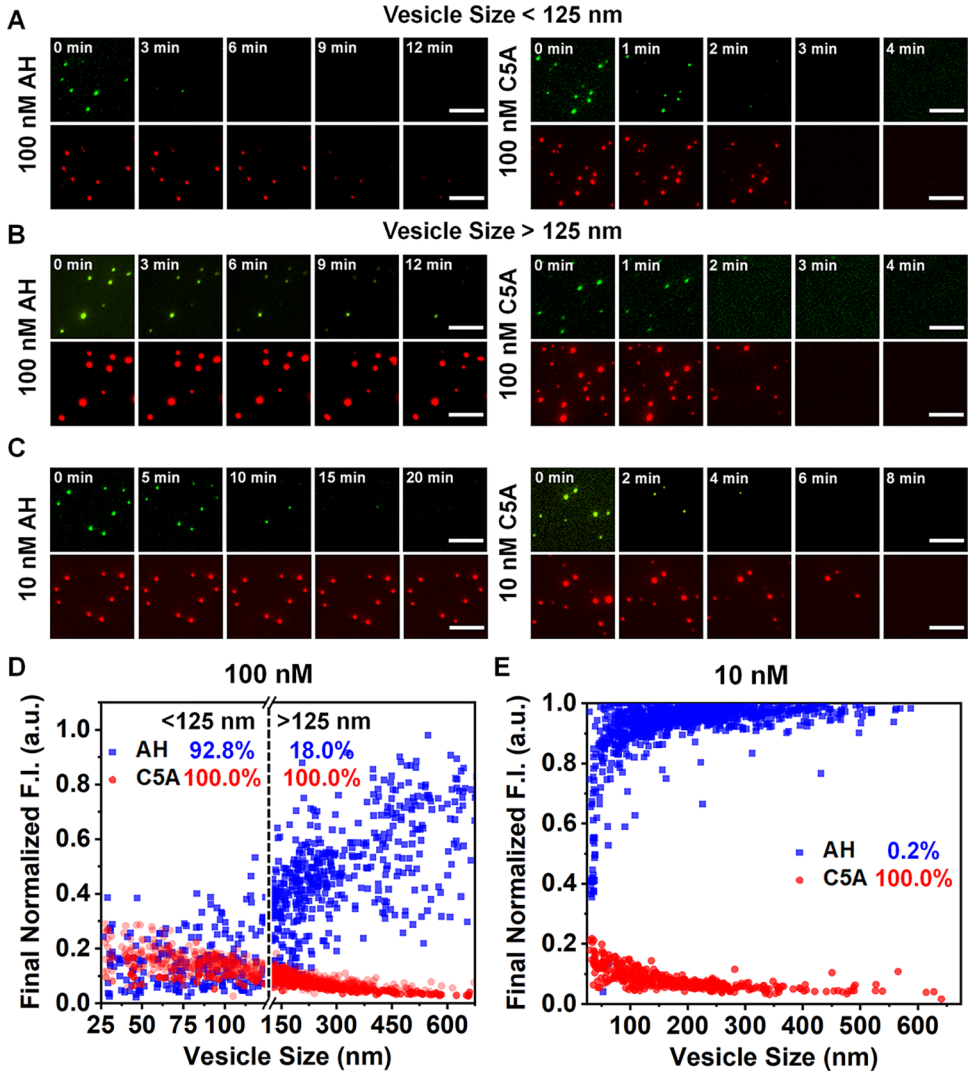


**Figure 3.** Distinct membrane-disruptive potencies of AH and C5A peptides. Time-lapsed fluorescence microscopy images of encapsulated calcein (green, top) and Rh-PE (red, bottom) dye probes for addition of 100 nM peptide to (A) small vesicles (<125 nm diameter) and (B) large vesicles (>125 nm diameter), or (C) 10 nM peptide to small vesicles (<125 nm diameter). Scale bars are 10 $\mu$m. (D, E) Corresponding single-vesicle data of peptide-induced vesicle rupture as a function of vesicle size, based on the rhodamine signal. Rupture is defined as when the final fluorescence intensity value of an individual vesicle was 30% or less of the original fluorescence intensity value of that vesicle. Each data point represents an individual vesicle.

C5A peptide are similar and endow the two peptides with similar physicochemical properties as well.

We next conducted lipid concentration-dependent CD spectroscopy experiments in order to measure the change in peptide secondary structure when peptide molecules partition from aqueous buffer solution into lipid membrane environments. This titration method also allowed us to identify how many lipid molecules are needed to interact with one peptide molecule in order to induce a stable $\alpha$-helical conformation. Typically, amphipathic peptide molecules exhibit increased helicity in lipid membrane environments, and the magnitude of the helicity change provides insight into the free energy of membrane partitioning.[51,52] In the free state, both peptides exhibited partial $\alpha$-helical structures in aqueous buffer solution due to the competition between intramolecular peptide hydrogen bonds and intermolecular binding to solvent molecules (Figures 2C,D).[53] In lipid membrane environments, both peptides transitioned from a polar (solvent) to a nonpolar (lipid membrane) environment, and this transition coincided with a change in the peptide secondary structure from a partial helix to an increased $\alpha$-helical conformation that was visible in the CD spectra. Helix stabilization is a common element of membrane−peptide interactions, and the folded structure of a peptide molecule in a lipid membrane environment has a lower free energy (more stable) than the less-folded structure in bulk solution; the degree of helicity has also been shown to be related to the extent of permeabilization activity.[54−56]

With increasing lipid concentration (in the range 0−2000 $\mu$M), the $\alpha$-helical character of peptides was greater because more peptide molecules partitioned into the lipid membrane environment until saturation was reached. For the AH peptide, the helicity increased from 39% in aqueous buffer to 71% at high lipid concentrations, and helix stabilization was reached at a peptide-to-lipid (P:L) ratio of about 1:10. By contrast, for the C5A peptide, the helicity increased from 32% in aqueous buffer to 88% at high lipid concentrations, and helix stabilization was reached at a P:L ratio of about 1:6.



DOI: 10.1021/acs.langmuir.9b01052
Langmuir 2019, 35, 9934−9943

Together, the data indicate that the C5A peptide achieves more extensive helix stabilization in lipid membrane environments than AH peptide. C5A helix stabilization also occurs at a smaller P:L ratio, which is consistent with its greater membrane partitioning, and the combination of these findings supports that the C5A peptide has greater interfacial activity against lipid membranes and is more potent than the AH peptide at lower P:L ratios.

For both peptides, we also investigated the ratio of the magnitudes of the two bands at the 208 and 222 nm wavelength positions, respectively (defined as $[\theta]_{222}/[\theta]_{208}$). Depending on the value of the ratio, it can be ascertained whether the peptides exist in a coiled-coil structure ($\gg$1) or as noninteracting helices ($\approx$1).[57] When the AH peptide was in aqueous buffer, the ratio was 3.5, which indicates that peptide molecules exist as a coiled-coil structure (Figure S2). In the presence of increasing lipid concentrations, the $[\theta]_{222}/[\theta]_{208}$ ratio decreased to around 1.1, which is more consistent with the value expected for noninteracting, linear helices rather than coiled-coil structures. By contrast, the C5A peptide existed predominantly as noninteracting monomers in buffer solution, and the ratio reached ~1.0 in the presence of higher lipid concentrations. The results support that the AH peptide transitions from a coiled-coil helical structure to a noninteracting, helical structure in the presence of lipid membrane environments while the C5A peptide exists as noninteracting helices in both aqueous buffer and lipid membrane environments. Collectively, the findings support that AH and C5A peptides have distinct conformational changes associated with membrane partitioning, and such factors help to explain why the two peptides have different potencies.

**Real-Time Tracking of Peptide-Induced Vesicle Rupture.** To directly track membrane–peptide interactions, we conducted time-lapsed fluorescence microscopy experiments in a microfluidic chamber whereby the peptide-mediated rupture of individual, tethered lipid vesicles on a functionalized glass surface was monitored in real-time. The vesicles were labeled with two fluorescence probes: a water-soluble calcein dye (green) was encapsulated in the vesicle interior, and a rhodamine dye-labeled phospholipid Rh-PE (red) was incorporated into the vesicle bilayer in order to track membrane permeabilization and lysis, respectively. The two types of membrane-interaction events were detected on the single-vesicle level on the basis of monitoring decreases in the intensity of the two fluorescence signals per individual vesicle, and over 300 vesicles could be monitored simultaneously per experiment.

For small vesicles (<125 nm diameter), 100 nM AH peptide ruptured nearly all vesicles within around 12 min while 100 nM C5A peptide ruptured all vesicles within only 3 min (Figure 3A). By contrast, for larger vesicles (>125 nm diameter), 100 nM AH peptide only ruptured a minor fraction of vesicles and most tethered vesicles remained intact (Figure 3B). On the other hand, 100 nM C5A peptide was still active against larger vesicles and ruptured them within 3 min. At 10 nM peptide concentration, the AH peptide lost membrane-disruptive activity against even small vesicles (<125 nm diameter) whereas the C5A peptide maintained similar activity levels and caused vesicle rupture within ~10 min (Figure 3C).

We also plotted the final intensity values of the rhodamine signal per individual vesicle versus each individual vesicle's size in order to quantitatively determine what fraction of vesicles was "ruptured" in different size categories.[58] For 100 nM AH peptide, 92.8% of small vesicles (<125 nm diameter) were ruptured while only 18.0% of larger vesicles were ruptured (>125 nm diameter) (Figure 3D). This vesicle size-dependent trend contrasted with the results obtained with 100 nM C5A peptide, in which case the peptide ruptured 100% of vesicles across the tested range of vesicle sizes. Strikingly, 10 nM AH peptide displayed negligible activity (0.2% rupture efficiency) against small vesicles (<125 nm diameter) whereas 10 nM C5A peptide still exhibited 100% rupture efficiency (Figure 3E).

Quantitative analysis of the vesicle rupture kinetics further confirmed that the C5A peptide is more potent (ruptures lipid vesicles at a 10-fold lower bulk peptide concentration than AH peptide) and causes membrane permeation and lysis on quicker time scales than AH peptide. Treatment with 100 nM AH peptide caused rapid permeabilization of small vesicles in around 2 min while membrane lysis typically occurred within 5 min (Figure 4A). However, 100 nM AH peptide caused much

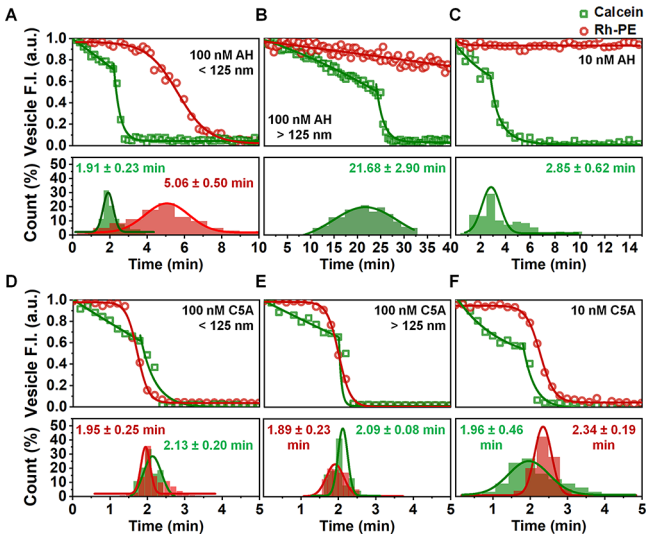


**Figure 4.** Change in normalized fluorescence intensity of individual, tethered vesicles as a result of membrane–peptide interactions. (A–F) Top: Representative profiles of single-vesicle rupture kinetics for AH and C5A peptides at different peptide concentrations and for different vesicle size ranges. Green and red colors denote calcein and rhodamine signals, respectively. Bottom: Corresponding histogram statistics of membrane permeabilization (green) and membrane lysis (red) time scales, where applicable.

slower permeabilization of larger vesicles without inducing membrane lysis (Figure 4B). Likewise, 10 nM AH peptide caused membrane permeabilization of smaller vesicles but did not cause membrane lysis (Figure 4C). As such, AH peptide-mediated pore formation is selective for small vesicles while a relatively high bulk peptide concentration is required to cause membrane lysis. By contrast, 100 nM C5A peptide is able to rapidly permeabilize and lyse both small and large vesicles on similar time scales of around 2 min (Figures 4D,E). Nearly identical results were obtained when 10 nM C5A peptide was added to small vesicles as well (Figure 4F). Thus, C5A peptide exhibits more potent, indiscriminate activity against lipid vesicles, as indicated by vesicle-independent rupture activity and rapid kinetics. Of particular note, the time scales of membrane permeabilization and membrane lysis were nearly identical for C5A peptide, suggesting that its membrane-interaction profile is distinct from that of AH peptide which


DOI: 10.1021/acs.langmuir.9b01052
Langmuir 2019, 35, 9934–9943

induces membrane lysis *after* a critical density of pores is formed. On the other hand, AH peptide exhibits vesicle size-dependent rupture activity, and the rate of membrane permeabilization is vesicle size-dependent as well, which is consistent with its known membrane curvature-sensitive, pore-forming behavior.

**Peptide-Induced Membrane Leakage.** To further investigate the effects of AH and C5A peptide treatment on membrane permeability, we conducted electrochemical impedance spectroscopy (EIS) measurements using a tethered bilayer lipid membrane (tBLM) platform. A schematic illustration of the measurement setup is presented in Figure 5A, and the experimental objective was to detect membrane

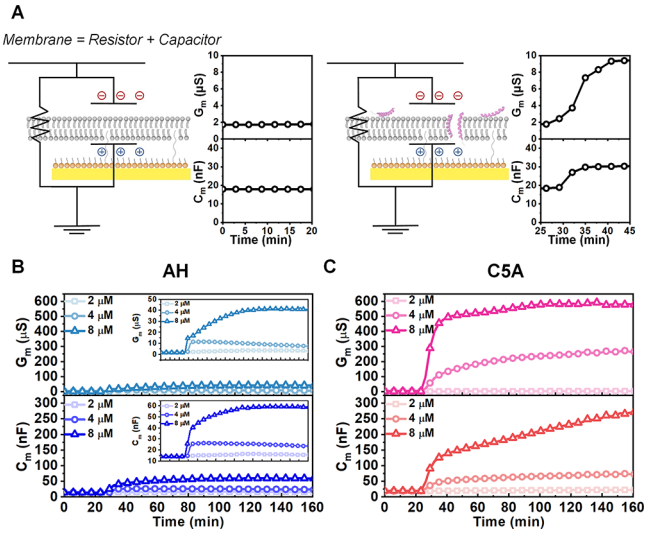


**Figure 5.** Electrochemical impedance spectroscopy analysis of membrane–peptide interactions involving AH and C5A peptides. (A) Schematic illustration of measurement setup. Peptide concentration-dependent changes in $G_m$ (top) and $C_m$ (bottom) signals as a function of time for (B) AH and (C) C5A peptides, respectively. Peptides were added at approximately $t$ = 20 min.

permeabilization based on ion leakage across the lipid bilayer. The setup measures the electrical conductance ($G_m$) across the tBLM, which is the inverse of its electrical resistance and expressed as $G_m = I/V$, where $I$ and $V$ are the current and voltage, respectively. The setup also measures the capacitance ($C_m$) of the tBLM, which signifies the magnitude of charged ions that are stored across the lipid bilayer and is expressed as $C_m = q/V$, where $q$ and $V$ are the charge and voltage, respectively. When membrane leakage occurs, the $G_m$ and $C_m$ values both increase (larger increases indicate greater membrane leakage) and a well-sealed tBLM is important for baseline stabilization. In our experiments, the tBLM was formed by rapid solvent exchange, and the initial $G_m$ and $C_m$ values were less than 2 $\mu$S and around 15–25 nF, respectively, which indicated good sealing properties.[59]

Figure 5B,C presents the concentration-dependent measurements results for AH and C5A peptides, respectively. Both peptides showed concentration-dependent membrane leakage activity, with distinct differences in the level of membrane permeabilization. At the highest test concentration, 8 $\mu$M AH peptide caused stable $G_m$ and $C_m$ shifts of around 40 $\mu$S and 60 nF, respectively. In marked contrast, 8 $\mu$M C5A peptide caused appreciably larger $G_m$ and $C_m$ shifts of around 550 $\mu$S and 270 nF, respectively, and the $C_m$ shift continued to increase over the measurement time period. The distinct membrane-interaction profiles are consistent with the AH peptide causing membrane thinning[60] while the C5A peptide exhibited more indiscriminate membrane solubilization, which bore resemblance to the behavior of sodium dodecyl sulfate (SDS) surfactant in terms of the extent of membrane disruption, albeit with slower kinetics (Figure S3). Together with the foregoing experimental data, the EIS results indicate that AH and C5A peptide have distinct membrane-interaction profiles that arise from unique conformational properties.

**Structural Modeling of Peptide Conformations.** To further evaluate the conformational properties of the two peptides, we modeled their secondary structures by performing computational simulations with the PEP-FOLD online server.[61,62] Figure 6A presents the simulated probabilities that the different amino positions are in helix, extended, or random conformations, as indicated by red, blue, and green colors, respectively. In general, it was predicted that both ends of the AH peptide have a high probability of helical conformation while it was predicted that the middle region of AH peptide (W9–18D) is likely nonhelical. On the other hand, the simulation results predicted that the C5A peptide has more uniform helical character throughout its amino acid sequence. On the basis of these predictions, the highest-ranking conformers of AH peptide mainly consisted of two helical regions that are separated by a nonhelical hinge in the middle (Figure 6B; see also Figures S4 and S5). This finding is consistent with the CD spectroscopy results indicating that the AH peptide likely has a coiled-coil structure, whereby the two helical regions of a peptide monomer interact and stabilize one another while the nonhelical hinge supports conformational freedom to minimize the peptide free energy. By contrast, the highest-ranking conformers of the C5A peptide have linear helix structures, which also agrees well with the CD spectroscopy results.

Taking into account the experimental and simulation results, our findings support that AH and C5A peptides exhibit distinct conformational properties that influence their membrane-disruptive activities, as presented in Figure 6C. While the AH peptide exhibits some degree of conformational flexibility in bulk solution, the simulation results indicate that it likely has two helical segments bifurcated by a flexible hinge, and this conformational arrangement offers insight into its empirically observed membrane curvature sensing properties. In high-curvature lipid membranes, there can be hydrophobic defects between neighboring lipid molecules,[63] and it appears that the AH peptide conformation is well-suited for fitting within these defects.

On the other hand, free C5A monomers exhibit lower helical character in the bulk solution while demonstrating greater membrane partitioning, as indicated by helix stabilization in the presence of lower total lipid concentrations in the CD spectroscopy experiments. As a result, the C5A peptide undergoes more extensive conformational changes, marked by a significant increase in helical character, upon membrane partitioning, which drives higher levels of interfacial activity.[56,64]

As such, the C5A peptide is less discriminate of lipid membrane properties, and there is a larger thermodynamic driving force to favor membrane partitioning. This finding explains why the C5A peptide is more potent than the AH peptide and interacts with lipid membrane via a distinct mechanism that is more akin to membrane solubilization than


DOI: 10.1021/acs.langmuir.9b01052
Langmuir 2019, 35, 9934–9943

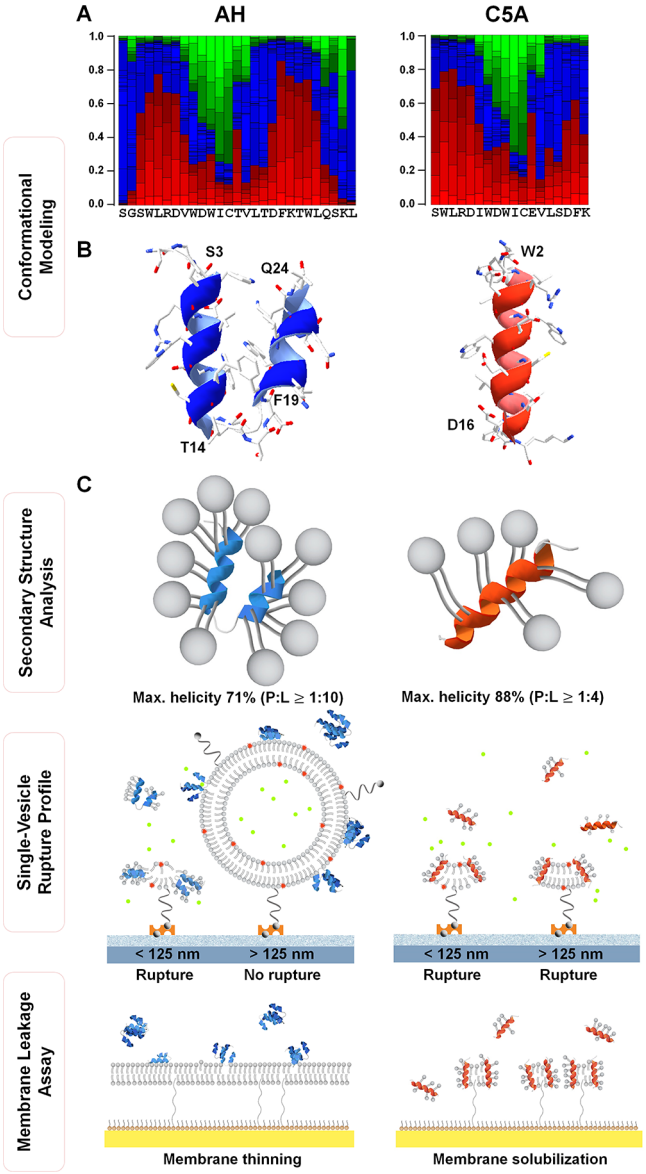


**Figure 6.** Structural modeling of AH and C5A peptides and implications for targeting selectivity. (A) Simulated probabilities of helical (red), extended (blue), and random (green) conformations are shown for each amino acid position in the peptide sequences. (B) Highest-ranking conformers of AH and C5A peptides are presented, pointing to distinct conformational properties of the two peptides in bulk solution. (C) Schematic illustration of how AH and C5A peptides interact with lipid membranes. Elements are not drawn to scale.

the curvature-sensitive pore formation exhibited by the AH peptide. Collectively, our findings reveal how the conformational properties of AH and C5A peptides influence structure–function relationships and help to explain the distinct membrane-interaction profiles of the two antiviral peptides. From a structural perspective, such information also provides a starting point to engineer antiviral peptides with desirable conformational properties and to screen candidate amino acid sequences using *in silico* methods and surface-sensitive measurement strategies. Looking forward, it will also be useful to apply this integrative approach across experiments and computational simulations to characterize the interactions of membrane-active peptides and other compounds with complex lipid membrane models and in conjunction with other surface-sensitive measurement techniques as well.[65,66]

## ■ ASSOCIATED CONTENT

### Supporting Information

The Supporting Information is available free of charge on the ACS Publications website at DOI: 10.1021/acs.langmuir.9b01052.

Additional information is provided about dynamic light scattering experiments (Figure S1), circular dichroism spectroscopy experiments and data analysis (Figure S2), electrochemical impedance spectroscopy experiments (Figure S3), and structural modeling simulations (Figures S4 and S5) (PDF)

## ■ AUTHOR INFORMATION


### Corresponding Author

*E-mail: njcho@ntu.edu.sg.

### ORCID

Soohyun Park: 0000-0003-3261-7585
Joshua A. Jackman: 0000-0002-1800-8102
Nam-Joon Cho: 0000-0002-8692-8955


### Notes

The authors declare the following competing financial interest(s): N.-J.C. is a co-inventor on US patent no. 8,728,793 that is related to the application of AH peptide molecules for antiviral therapy. The other authors declare no competing interests.

## ■ ACKNOWLEDGMENTS

The authors thank Dr. Bruce Cornell for stimulating discussions. This work was supported by the National Research Foundation of Singapore through a Competitive Research Programme grant (NRF-CRP10-2012-07) and a Proof-of-Concept grant (NRF2015NRF-POC0001-19). Additional support was provided by the Creative Materials Discovery Program through the National Research Foundation of Korea funded by the Ministry of Science, ICT and Future Planning (NRF-2016M3D1A1024098).

## ■ REFERENCES


(1) Zasloff, M. Antimicrobial Peptides of Multicellular Organisms. *Nature* **2002**, *415* (6870), 389–395.

(2) Hancock, R. E.; Sahl, H.-G. Antimicrobial and Host-Defense Peptides as New Anti-Infective Therapeutic Strategies. *Nat. Biotechnol.* **2006**, *24* (12), 1551.

(3) Guha, S.; Ghimire, J.; Wu, E.; Wimley, W. C. Mechanistic Landscape of Membrane-Permeabilizing Peptides. *Chem. Rev.* **2019**, *119*, 6040.

(4) Brogden, K. A. Antimicrobial Peptides: Pore Formers or Metabolic Inhibitors in Bacteria? *Nat. Rev. Microbiol.* **2005**, 3 (3), 238.

(5) Melo, M. N.; Ferre, R.; Castanho, M. A. Antimicrobial Peptides: Linking Partition, Activity and High Membrane-Bound Concentrations. *Nat. Rev. Microbiol.* **2009**, *7* (3), 245.

(6) Badani, H.; Garry, R. F.; Wimley, W. C. Peptide Entry Inhibitors of Enveloped Viruses: The Importance of Interfacial Hydrophobicity. *Biochim. Biophys. Acta, Biomembr.* **2014**, *1838* (9), 2180–2197.

(7) Vigant, F.; Santos, N. C.; Lee, B. Broad-Spectrum Antivirals Against Viral Fusion. *Nat. Rev. Microbiol.* **2015**, *13* (7), 426–437.

(8) Jackman, J. A.; Shi, P.-Y.; Cho, N.-J. Targeting the Achilles Heel of Mosquito-Borne Viruses for Antiviral Therapy. *ACS Infect. Dis.* **2019**, *5*, 4.




DOI: 10.1021/acs.langmuir.9b01052
*Langmuir* 2019, 35, 9934–9943

(9) Thormar, H.; Isaacs, C. E.; Brown, H. R.; Barshatzky, M. R.; Pessolano, T. Inactivation of Enveloped Viruses and Killing of Cells by Fatty Acids and Monoglycerides. *Antimicrob. Agents Chemother.* **1987**, *31* (1), 27−31.
(10) Vollenbroich, D.; Özel, M.; Vater, J.; Kamp, R. M.; Pauli, G. Mechanism of Inactivation of Enveloped Viruses by the Biosurfactant Surfactin from Bacillus Subtilis. *Biologicals* **1997**, *25* (3), 289−297.
(11) Sands, J.; Auperin, D.; Snipes, W. Extreme Sensitivity of Enveloped Viruses, Including Herpes Simplex, to Long-Chain Unsaturated Monoglycerides and Alcohols. *Antimicrob. Agents Chemother.* **1979**, *15* (1), 67−73.
(12) Vigant, F.; Hollmann, A.; Lee, J.; Santos, N. C.; Jung, M. E.; Lee, B. The Rigid Amphipathic Fusion Inhibitor dUY11 Acts Through Photosensitization of Viruses. *J. Virol.* **2014**, *88* (3), 1849−1853.
(13) Jackman, J. A.; Costa, V. V.; Park, S.; Real, A. L. C.; Park, J. H.; Cardozo, P. L.; Ferhan, A. R.; Olmo, I. G.; Moreira, T. P.; Bambirra, J. L.; et al. Therapeutic Treatment of Zika Virus Infection Using a Brain-Penetrating Antiviral Peptide. *Nat. Mater.* **2018**, *17* (11), 971.
(14) Veazey, R. S.; Chatterji, U.; Bobardt, M.; Russell-Lodrigue, K. E.; Li, J.; Wang, X.; Gallay, P. A. C5A Protects Macaques from Vaginal Simian-Human Immunodeficiency Virus Challenge. *Antimicrob. Agents Chemother.* **2016**, *60* (1), 693−698.
(15) Jackman, J. A.; Saravanan, R.; Zhang, Y.; Tabaei, S. R.; Cho, N. J. Correlation Between Membrane Partitioning and Functional Activity in a Single Lipid Vesicle Assay Establishes Design Guidelines for Antiviral Peptides. *Small* **2015**, *11* (20), 2372−2379.
(16) Aloia, R. C.; Tian, H.; Jensen, F. C. Lipid Composition and Fluidity of the Human Immunodeficiency Virus Envelope and Host Cell Plasma Membranes. *Proc. Natl. Acad. Sci. U. S. A.* **1993**, *90* (11), 5181−5185.
(17) Cheng, G.; Montero, A.; Gastaminza, P.; Whitten-Bauer, C.; Wieland, S. F.; Isogawa, M.; Fredericksen, B.; Selvarajah, S.; Gallay, P. A.; Ghadiri, M. R.; Chisari, F. V. A Virocidal Amphipathic $\alpha$-Helical Peptide that Inhibits Hepatitis C Virus Infection In Vitro. *Proc. Natl. Acad. Sci. U. S. A.* **2008**, *105* (8), 3088−3093.
(18) Elazar, M.; Cheong, K. H.; Liu, P.; Greenberg, H. B.; Rice, C. M.; Glenn, J. S. Amphipathic Helix-Dependent Localization of NS5A Mediates Hepatitis C Virus RNA Replication. *J. Virol.* **2003**, *77* (10), 6055−6061.
(19) Huang, L.; Sineva, E. V.; Hargittai, M. R.; Sharma, S. D.; Suthar, M.; Raney, K. D.; Cameron, C. E. Purification and Characterization of Hepatitis C Virus Non-Structural Protein 5A Expressed in Escherichia Coli. *Protein Expression Purif.* **2004**, *37* (1), 144−153.
(20) Love, R. A.; Brodsky, O.; Hickey, M. J.; Wells, P. A.; Cronin, C. N. Crystal Structure of a Novel Dimeric Form of NS5A Domain I Protein From Hepatitis C Virus. *J. Virol.* **2009**, *83* (9), 4395−4403.
(21) Tellinghuisen, T. L.; Marcotrigiano, J.; Rice, C. M. Structure of the Zinc-Binding Domain of an Essential Component of the Hepatitis C Virus Replicase. *Nature* **2005**, *435* (7040), 374.
(22) Cho, N.-J.; Cheong, K. H.; Lee, C.; Frank, C. W.; Glenn, J. S. Binding Dynamics of Hepatitis C Virus' NS5A Amphipathic Peptide to Cell and Model Membranes. *J. Virol.* **2007**, *81* (12), 6682−6689.
(23) Jackman, J. A.; Cho, N.-J. Model Membrane Platforms for Biomedicine: Case Study on Antiviral Drug Development. *Biointerphases* **2012**, *7* (1), 18.
(24) Cho, N.-J.; Lee, C.; Pang, P. S.; Pham, E. A.; Fram, B.; Nguyen, K.; Xiong, A.; Sklan, E. H.; Elazar, M.; Koytak, E. S.; et al. Phosphatidylinositol 4, 5-Bisphosphate is an HCV NS5A Ligand and Mediates Replication of the Viral Genome. *Gastroenterology* **2015**, *148* (3), 616−625.
(25) Cho, N.-J.; Dvory-Sobol, H.; Xiong, A.; Cho, S.-J.; Frank, C. W.; Glenn, J. S. Mechanism of an Amphipathic $\alpha$-Helical Peptide's Antiviral Activity Involves Size-Dependent Virus Particle Lysis. *ACS Chem. Biol.* **2009**, *4* (12), 1061−1067.
(26) Jackman, J. A.; Zan, G. H.; Zhdanov, V. P.; Cho, N.-J. Rupture of Lipid Vesicles by a Broad-Spectrum Antiviral Peptide: Influence of Vesicle Size. *J. Phys. Chem. B* **2013**, *117* (50), 16117−16128.
(27) Cho, N.-J.; Cho, S.-J.; Cheong, K. H.; Glenn, J. S.; Frank, C. W. Employing an Amphipathic Viral Peptide to Create a Lipid Bilayer on Au and TiO2. *J. Am. Chem. Soc.* **2007**, *129* (33), 10050−10051.
(28) Jackman, J. A.; Goh, H. Z.; Zhdanov, V. P.; Knoll, W.; Cho, N.-J. Deciphering How Pore Formation Causes Strain-Induced Membrane Lysis of Lipid Vesicles. *J. Am. Chem. Soc.* **2016**, *138* (4), 1406−1413.
(29) Zan, G. H.; Jackman, J. A.; Cho, N.-J. AH Peptide-Mediated Formation of Charged Planar Lipid Bilayers. *J. Phys. Chem. B* **2014**, *118* (13), 3616−3621.
(30) Jackman, J. A.; Linardy, E.; Yoo, D.; Seo, J.; Ng, W. B.; Klemme, D. J.; Wittenberg, N. J.; Oh, S. H.; Cho, N. J. Plasmonic Nanohole Sensor for Capturing Single Virus-Like Particles toward Virucidal Drug Evaluation. *Small* **2016**, *12* (9), 1159−1166.
(31) Bobardt, M. D.; Cheng, G.; de Witte, L.; Selvarajah, S.; Chatterji, U.; Sanders-Beer, B. E.; Geijtenbeek, T. B.; Chisari, F. V.; Gallay, P. A. Hepatitis C virus NS5A Anchor Peptide Disrupts Human Immunodeficiency Virus. *Proc. Natl. Acad. Sci. U. S. A.* **2008**, *105* (14), 5525−5530.
(32) De Witte, L.; Bobardt, M. D.; Chatterji, U.; Van Loenen, F. B.; Verjans, G. M.; Geijtenbeek, T. B.; Gallay, P. A. HSV Neutralization by the Microbicidal Candidate C5A. *PLoS One* **2011**, *6* (5), No. e18917.
(33) Denton, P. W.; Othieno, F.; Martinez-Torres, F.; Zou, W.; Krisko, J. F.; Fleming, E.; Zein, S.; Powell, D. A.; Wahl, A.; Kwak, Y. T.; et al. One Percent Tenofovir Applied Topically to Humanized BLT Mice and Used According to the CAPRISA 004 Experimental Design Demonstrates Partial Protection from Vaginal HIV Infection, Validating the BLT Model for Evaluation of New Microbicide Candidates. *J. Virol.* **2011**, *85* (15), 7582−7593.
(34) Lin, Q.; Fang, D.; Hou, X.; Le, Y.; Fang, J.; Wen, F.; Gong, W.; Chen, K.; Wang, J. M.; Su, S. B. HCV Peptide (C5A), an Amphipathic $\alpha$-Helical Peptide of Hepatitis Virus C, is an Activator of N-Formyl Peptide Receptor in Human Phagocytes. *J. Immunol.* **2011**, *186* (4), 2087−2094.
(35) Smith, D. B.; Bukh, J.; Kuiken, C.; Muerhoff, A. S.; Rice, C. M.; Stapleton, J. T.; Simmonds, P. Expanded Classification of Hepatitis C Virus Into 7 Genotypes and 67 Subtypes: Updated Criteria and Genotype Assignment Web Resource. *Hepatology* **2014**, *59* (1), 318−327.
(36) Zein, N. N. Clinical Significance of Hepatitis C Virus Genotypes. *Clin. Microbiol. Rev.* **2000**, *13* (2), 223−235.
(37) Ariga, K.; Mori, T.; Li, J. Langmuir Nanoarchitectonics From Basic to Frontier. *Langmuir* **2019**, *35*, 3585.
(38) Komiyama, M.; Mori, T.; Ariga, K. Molecular Imprinting: Materials Nanoarchitectonics With Molecular Information. *Bull. Chem. Soc. Jpn.* **2018**, *91* (7), 1075−1111.
(39) Yoon, B. K.; Jackman, J. A.; Park, S.; Mokrzecka, N.; Cho, N.-J. Characterizing the Membrane-Disruptive Behavior of Dodecylglycerol Using Supported Lipid Bilayers. *Langmuir* **2019**, *35*, 3568.
(40) Komiyama, M.; Yoshimoto, K.; Sisido, M.; Ariga, K. Chemistry Can Make Strict and Fuzzy Controls for Bio-Systems: DNA Nanoarchitectonics and Cell-Macromolecular Nanoarchitectonics. *Bull. Chem. Soc. Jpn.* **2017**, *90* (9), 967−1004.
(41) Edelhoch, H. Spectroscopic Determination of Tryptophan and Tyrosine in Proteins. *Biochemistry* **1967**, *6* (7), 1948−1954.
(42) Ladokhin, A. S.; Fernández-Vidal, M.; White, S. H. CD Spectroscopy of Peptides and Proteins Bound to Large Unilamellar Vesicles. *J. Membr. Biol.* **2010**, *236* (3), 247−253.
(43) Morrisett, J. D.; David, J. S. K.; Pownall, H. J.; Gotto, A. M. Interaction of an Apolipoprotein (apoLP-alanine) with Phosphatidylcholine. *Biochemistry* **1973**, *12* (7), 1290−1299.
(44) MacDonald, R. C.; MacDonald, R. I.; Menco, B. P. M.; Takeshita, K.; Subbarao, N. K.; Hu, L.-r. Small-Volume Extrusion Apparatus for Preparation of Large, Unilamellar Vesicles. *Biochim. Biophys. Acta, Biomembr.* **1991**, *1061* (2), 297−303.
(45) Tabaei, S. R.; Rabe, M.; Zhdanov, V. P.; Cho, N.-J.; Höök, F. Single Vesicle Analysis Reveals Nanoscale Membrane Curvature


DOI: 10.1021/acs.langmuir.9b01052
*Langmuir* 2019, 35, 9934−9943

Selective Pore Formation in Lipid Membranes by an Antiviral α-Helical Peptide. *Nano Lett.* **2012**, *12* (11), 5719−5725.
(46) Cranfield, C.; Carne, S.; Martinac, B.; Cornell, B. The Assembly and Use of Tethered Bilayer Lipid Membranes (tBLMs). In *Methods in Membrane Lipids*; Springer, 2015; pp 45−53.
(47) Chilambi, G. S.; Gao, I. H.; Yoon, B. K.; Park, S.; Kawakami, L. M.; Ravikumar, V.; Chan-Park, M. B.; Cho, N.-J.; Bazan, G. C.; Kline, K. A.; Rice, S. A.; Hinks, J. Membrane Adaptation Limitations in Enterococcus Faecalis Underlie Sensitivity and the Inability to Develop Significant Resistance to Conjugated Oligoelectrolytes. *RSC Adv.* **2018**, *8* (19), 10284−10293.
(48) Lamiable, A.; Rey, J.; Vavrusa, M.; Derreumaux, P.; Thévenet, P.; Tufféry, P. PEP-FOLD3: Faster de novo Structure Prediction for Linear Peptides in Solution and in Complex. *Nucleic Acids Res.* **2016**, *44* (W1), W449−W454.
(49) Maupetit, J.; Tuffery, P.; Derreumaux, P. A Coarse-Grained Protein Force Field for Folding and Structure Prediction. *Proteins: Struct., Funct., Genet.* **2007**, *69* (2), 394−408.
(50) Guex, N.; Peitsch, M. C. SWISS-MODEL and the Swiss-Pdb Viewer: An Environment for Comparative Protein Modeling. *Electrophoresis* **1997**, *18* (15), 2714−2723.
(51) Wang, Y.; Chen, C. H.; Hu, D.; Ulmschneider, M. B.; Ulmschneider, J. P. Spontaneous Formation of Structurally Diverse Membrane Channel Architectures From a Single Antimicrobial Peptide. *Nat. Commun.* **2016**, *7*, 13535.
(52) Wieprecht, T.; Apostolov, O.; Beyermann, M.; Seelig, J. Thermodynamics of the α-Helix-Coil Transition of Amphipathic Peptides in a Membrane Environment: Implications for the Peptide-Membrane Binding Equilibrium. *J. Mol. Biol.* **1999**, *294* (3), 785−794.
(53) White, S. H.; Wimley, W. C.; Ladokhin, A. S.; Hristova, K. Energetics of Peptide−Bilayer Interactions. *Methods Enzymol.* **1998**, *295*, 62−87.
(54) White, S. H.; Wimley, W. C.; Ladokhin, A. S.; Hristova, K. Protein Folding in Membranes: Determining Energetics of Peptide-Bilayer Interactions. *Methods Enzymol.* **1998**, *295*, 62−87.
(55) Shai, Y. Mechanism of the Binding, Insertion and Destabilization of Phospholipid Bilayer Membranes by α-Helical Antimicrobial and Cell Non-Selective Membrane-Lytic Peptides. *Biochim. Biophys. Acta, Biomembr.* **1999**, *1462* (1), 55−70.
(56) Krauson, A. J.; Hall, O. M.; Fuselier, T.; Starr, C. G.; Kauffman, W. B.; Wimley, W. C. Conformational Fine-Tuning of Pore-Forming Peptide Potency and Selectivity. *J. Am. Chem. Soc.* **2015**, *137* (51), 16144−16152.
(57) Pan, O. H.; Beck, K. The C-Terminal Domain of Matrilin-2 Assembles Into a Three-Stranded α-Helical Coiled Coil. *J. Biol. Chem.* **1998**, *273* (23), 14205−14209.
(58) Lohr, C.; Kunding, A. H.; Bhatia, V. K.; Stamou, D. Constructing size distributions of liposomes from single-object fluorescence measurements. *Methods Enzymol.* **2009**, *465*, 143−160.
(59) Al Khamici, H.; Hossain, K. R.; Cornell, B. A.; Valenzuela, S. M. Investigating Sterol and Redox Regulation of the Ion Channel Activity of CLIC1 Using Tethered Bilayer Membranes. *Membranes* **2016**, *6* (4), 51.
(60) Cho, N.-J.; Cho, S.-J.; Hardesty, J. O.; Glenn, J. S.; Frank, C. W. Creation of Lipid Partitions by Deposition of Amphipathic Viral Peptides. *Langmuir* **2007**, *23* (21), 10855−10863.
(61) Shen, Y.; Maupetit, J.; Derreumaux, P.; Tufféry, P. Improved PEP-FOLD Approach for Peptide and Miniprotein Structure Prediction. *J. Chem. Theory Comput.* **2014**, *10* (10), 4745−4758.
(62) Ciemny, M.; Kurcinski, M.; Kamel, K.; Kolinski, A.; Alam, N.; Schueler-Furman, O.; Kmiecik, S. Protein−Peptide Docking: Opportunities and Challenges. *Drug Discovery Today* **2018**, *23*, 1530.
(63) Hatzakis, N. S.; Bhatia, V. K.; Larsen, J.; Madsen, K. L.; Bolinger, P.-Y.; Kunding, A. H.; Castillo, J.; Gether, U.; Hedegård, P.; Stamou, D. How curved membranes recruit amphipathic helices and protein anchoring motifs. *Nat. Chem. Biol.* **2009**, *5* (11), 835−841.
(64) Hollmann, A.; Martínez, M.; Noguera, M. E.; Augusto, M. T.; Disalvo, A.; Santos, N. C.; Semorile, L.; Maffía, P. C. Role of Amphipathicity and Hydrophobicity in the Balance Between Hemolysis and Peptide−Membrane Interactions of Three Related Antimicrobial Peptides. *Colloids Surf., B* **2016**, *141*, 528−536.
(65) Lu, N.; Yang, K.; Yuan, B.; Ma, Y. Molecular Response and Cooperative Behavior During the Interactions of Melittin with a Membrane: Dissipative Quartz Crystal Microbalance Experiments and Simulations. *J. Phys. Chem. B* **2012**, *116* (31), 9432−9438.
(66) Losada-Pérez, P.; Khorshid, M.; Hermans, C.; Robijns, T.; Peeters, M.; Jiménez-Monroy, K.; Truong, L.; Wagner, P. Melittin Disruption of Raft and Non-Raft-Forming Biomimetic Membranes: A Study by Quartz Crystal Microbalance With Dissipation Monitoring. *Colloids Surf., B* **2014**, *123*, 938−944.



DOI: 10.1021/acs.langmuir.9b01052
*Langmuir* 2019, 35, 9934−9943